Analytica Chimica Acta 1110 (2020) 56–63

Contents lists available at ScienceDirect

Analytica Chimica Acta

journal homepage: www.elsevier.com/locate/aca

Core-satellite assemblies and exonuclease assisted double amplification strategy for ultrasensitive SERS detection of biotoxin

Dandan Huang [a, 1], Jiaming Chen [a, 1], Li Ding [a], Longhua Guo [b, *], Palanisamy Kannan [b, **], Fang Luo [a], Bin Qiu [a], Zhenyu Lin [a, ***]

[a] Ministry of Education Key Laboratory for Analytical Science of Food Safety and Biology, Fujian Provincial Key Laboratory of Analysis and Detection for Food Safety, College of Chemistry, Fuzhou University, Fuzhou, Fujian, 350116, China
[b] College of Biological, Chemical Sciences and Engineering, Jiaxing University, Jiaxing, 314001, China

HIGHLIGHTS

- We report a double amplification strategy for the ultrasensitive detection of biotoxin.
- Exonuclease III -assisted efficient recycling is utilized for signal amplification.
- Core-satellite assembly produced numerous "*hot spots*" effectively enhances the SERS signals.
- The detection OTA in red wine is demonstrated with the RSD of 6.08 −8.61%.
- The limit of detection of the proposed sensor is 0.83 fg mL^{-1} (S/N = 3) for OTA.

GRAPHICAL ABSTRACT

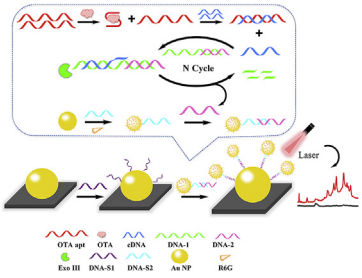

ARTICLE INFO

Article history:
Received 2 February 2020
Received in revised form
24 February 2020
Accepted 26 February 2020
Available online 28 February 2020

Keywords:
Core-satellite assemblies
Signal amplification
Surface-enhanced Raman scattering
Biotoxin
Red wine

ABSTRACT

In this work, core-satellite assemblies and exonuclease assisted double amplification strategy is developed to produce surface-enhanced Raman scattering (SERS) biosensor towards ultrasensitive detection of biotoxin. In the presence of target molecules, the exonuclease III (Exo III) assisted efficient recycling amplification provides an excellent pathway for the fabrication of core-satellite SERS sensor. Briefly, the proposed strategy includes the following double amplifications: (i) Exo III induced target-related signal amplification; (ii) core-satellite assemblies assisted formation of SERS "hot-spots" induced signal amplification. To show the applicability of the suggested strategy, the detection of ochratoxin A (OTA), one of the most toxic and widely distributed biotoxin, is demonstrated as an example. The results show that the limit of detection (LOD) of OTA is 0.83 fg mL^{-1} (S/N = 3). On the basis of the DNA aptamer induced specific target recognition, hence our sensing strategy is easy to be expended to the ultrasensitive detection of other targets, e.g., DNAs, RNAs, and other molecules that have corresponding DNA aptamers.

* Corresponding author. Ministry of Education Key Laboratory for Analytical Science of Food Safety and Biology, Fujian Provincial Key Laboratory of Analysis and Detection for Food Safety, College of Chemistry, Fuzhou University, Fuzhou, Fujian, 350116, China.
** Corresponding author.
*** Corresponding author.
E-mail addresses: guolh@zjxu.edu.cn (L. Guo), ktpkannan@mail.zjxu.edu.cn (P. Kannan), zylin@fzu.edu.cn (Z. Lin).
[1] These authors contributed equally to this work.

https://doi.org/10.1016/j.aca.2020.02.058
0003-2670/

1. Introduction

Surface-enhanced Raman scattering (SERS) is a surface-sensitive science, it can vastly enhance the Raman signal of analytes adsorbed or located at close to metallic nanostructures [1]. SERS based detection strategies have received significant attention because of its vast advantages including rapid detection time, high accuracy, sensitivity, and selectivity. The enhancement of SERS signals is mainly due to the excitation of localized surface plasmon resonance (LSPR) via the amplified local electromagnetic (EM) field effect [2–4]. Notably, the enhanced SERS enhancement factors (EF) were observed in "hot spot" areas of the junction between the two nanostructured particles [5–8]. It has already proved that powerful coupled plasmonic assemblies have shown a strong electromagnetic "hot spots", which yielded extraordinary EF in SERS based detections [9–13]. For instance, a SERS sensor based detection of AFB1 was proposed using heterogeneous gold nanostar core-silver nanoparticle satellite assemblies [14]. The SERS signal was enhanced through the formation of gold (Au) nanostar core-silver (Ag) nanoparticle satellite assemblies. When AFB1 was introduced into the system, the Ag satellite was then removed gradually; as a result, the SERS signals were decreased with respect to the concentration of AFB1. Besides, Ag NPs pyramids of DNA-driven self-assembly could be changed due the formation of a shorter gap distance of Ag NPs, which produced tremendous "*hot spots*" while introducing target molecules [15]. This powerful SERS technique potentially used to detect biomolecules or toxins as low as attomolar (aM) for clinical and food safety applications.

Exonuclease III (Exo III) is a key exodeoxyribonuclease enzymatic substance. It can selectively catalyze the progressive removal of one strand with either 3′ a blunt or overhang end in the duplex DNA. In addition, Exo III has no effect on double-stranded DNA at 3' overhangs of the DNA sequence of four or more bases. Typically, this foreseeable selectivity of Exo III makes the intact DNA strand to be recycled as target sequence in exonuclease reaction [16]. Further, it can be used as a valid catalytic element for amplified DNA detection, which resulting in prominent enhancement of detectable signals with high sensitivity, and selectivity.

Fungi play an extensive role in decomposition of fruits, vegetables, and food materials due to their pathogenic nature to the harvested products. Ochratoxin A (OTA), a well-known extremely toxic mycotoxins, produced by Aspergillus and Penicillium fungi species, has received tremendous attention in health and food safety [17,18]. OTA contaminates wide variety of agricultural products such as rice, wheat, maize, coffee, and peanut, which outcomes severe health issues through food chain process including hepatotoxic, nephrotoxic, teratogenic, neurotoxic, and immuno-toxic problems [19–24]. The International Agency for Research on Cancer (IARC) has classified OTA as group 2B of possible human carcinogen [25]. European Commission also regulates limits for OTA in food products such as roasted coffee (5 $\mu g\ kg^{-1}$), dried fruits (10 $\mu g\ kg^{-1}$), raw cereal grains (5 $\mu g\ kg^{-1}$), and wines (2 $\mu g\ kg^{-1}$) [26]. Thus, the ultrasensitive detection of OTA in food matrix is of great significance in clinical and health viewpoints. Over the past few years, a lot of methods have been exploited to detect accurate concentration of OTA. In particular, traditional OTA detection methods include liquid chromatography combined with mass spectrometry (LC-MS), high-performance liquid chromatography (HPLC), and antibody based techniques have been reported, though these methods are time-consuming, expensive and depend on the skilled worker for its operations [27–29]. Most of the reported methods for detecting biotoxin using the SERS technology have involved corresponding aptamers. Aptamer is used to solve the problem of SERS detection selectivity. Ganbold Erdene-Ochir et al. [30] proposed a method for detecting OTA based on the different absorption resolution of OTA aptamer labeled with Cy5 Raman reporter molecules. The aptamer is easily absorbed on the surface of Ag nanoparticles, which generates a strong SERS signal. In the presence of OTA, this binding is hindered and the SERS signal is weakened to achieve the purpose of detecting OTA. Zhao Yuan et al. [31] embedded Raman reporter molecules into the Ag @ Au CS NPs, and the aptamer of the biotoxin molecule was connected to the surface of Ag @ Au CS NPs. When there is no target, the aptamer is complementary paired with cDNA on the surface of the magnetic bead, and there is still a SERS signal after washing; when the target is present, the target binds to the aptamer, and Ag @ Au CS NPs is separated from the magnetic beads. The SERS signal weakened after washing. Song dan et al. [32] also used a similar method by combining Fe3O4 @ Au magnetic nanoparticles and Au-DTNB @ Ag nanoprobes under the pairing action of the biotoxin aptamer and its complementary strand, and then adding the target to separate them, which causes the SER signal to weaken.

In this study, we report core-satellite assemblies and exonuclease assisted double amplification strategy for high selective and ultrasensitive SERS detection of OTA. The core-satellite nanostructures are constructed taking DNA as the linker, thus the aptamer would bind with OTA and cause efficient Exo III recycling amplification process. In particular, the concentration of OTA determines effective formation of core-satellite assemblies via reducing the gap length of the Au NPs, which results in enhanced SERS signals for detecting OTA. On account of the experimental outcomes, we propose that the core-satellite structures and Exo III assisted double amplification strategy based sensing platform is considered as potential tool for clinical and food safety applications.

2. Material and methods

2.1. Reagents and materials

All oligonucleotides sequences were as follows (>97%, Shanghai Sangon Biotechnology Co., Ltd):

aptamer:5′-GAT CGG GTG TGG GTG GCG TAA AGG GAG CAT CGG ACA-3'.

cDNA:5′-ATG CTC CCT TTA CGC CAC CCA ACG GGT -3'.

DNA-1:5′-TAA CAG GAT TCG CAC GTC GTC GTG GCG TAA AGG GAG CAT-3'.

DNA-2:5′-GAC GAC GTG CGA ATC CTG AAT GCG-3′

DNA-S1:5′—SH—AAA AAA CGC ATT CAG GAT-3'.

DNA-S2:5′-TCG CAC GTC GTC—SH—3'.

Gold (III) chloride trihydrate ($HAuCl_4 \cdot 4H_2O$,99.9%) and sodium chloride (NaCl, >99.8%) were purchased from Sinopharm Chem. Re. Co., Ltd (Shanghai, China). Potassium chloride (KCl, 99.5%), magnesium chloride hexahydrate ($MgCl_2 \cdot 6H_2O$,99%), sodium citrate ($Na_3C_6H_5O_7 \cdot 2H_2O$,99.8%), (3-aminopropyl)triethoxysilane ($C_9H_{23}NO_3Si$,98%), mercaptosuccinic acid ($C_4H_6O_4S$, 98%, MSA), N-(3-dimethylaminopropyl)-N′-ethylcarbodiimide hydrochloride ($C_8H_{17}N_3 \cdot HCl$, 98%), DL-dithiothreitol (DTT, 99%), and tris(hydroxymethyl)aminomethane hydrochloride (Tris HCl, 99%) were obtained from Aladdin Company (Shanghai, China). mPEG-COOH (Mw ≈ 2000) was purchased from Xi'an ruixi Biological Technology Co., Ltd. Exonuclease III (Exo III) was obtained from Thermo Scientific Co., Ltd (Shanghai, China). The toxins used in the selective experiment, as well as OTA, were purchased from Sigma-Aldrich Chemical Co., Ltd. All other chemicals used in this work were analytical grade and used directly without further purification. All the experimental solutions were prepared from Milli-Q water (18.2 $M\Omega\ cm^{-1}$).

2.2. Synthesis of Au NPs

Au NPs were prepared on the basis of the modified Frens method [33,34]. Briefly, $HAuCl_4$ aqueous solution (100 mL 0.25 mM) was heated to 100 °C for 30 min under severe agitation. Then sodium citrate solution (10 mL 1%) was added into the boiling solution under continuous stirring. Color of the solution was changed to ruby red after 20 min. This indicates the formation of 25 nm sized Au NPs and the above solution was stored at 4 °C for further experimental use.

100 nm quasispherical Au NPs were prepared according to previous report [35]. The Au nanoseeds were synthesized by Frens method [33]. Next, $HAuCl_4$ aqueous solution (50 mL 0.25 mM) was heated to boiling with stirring. Then sodium citrate solution (1.75 mL 1%) was rapidly added to the above solution. The color of the solution changed to wine red, indicating the formation of Au nanoseeds, which was used for the further experiments. An aqueous solution containing $HAuCl_4$ (50 mL) and Au nanoseeds was stirred constantly, and then MSA was added. The above obtained Au NPs were used for the preparation of SERS substrates.

2.3. Preparation of SERS nanotag

Au NPs were modified with DNA-S2 at a molar ratio of 100:1, and the mixture was incubated overnight in 10 mM Tris-HCl buffer (10 mM $MgCl_2$, 50 mM NaCl and 10 mM KCl; pH 7.4) at 37 °C, and 1 M NaCl solution was gradually added to an ultimate concentration of 0.1 M. Then the mix was centrifuged (8000 rpm, 20 min), and the pellet was re-suspended in Tris-HCl buffer (10 mM). Raman reporter R6G, with a ultimate concentration of 100 μM, was dissolved in aqueous solution, added to Au NPs-DNA-S2 conjugates and incubated overnight at 37 °C. Afterwards, the mixture was washed by centrifuging (8000 rpm, 20 min) and re-dissolved in 10 mM Tris-HCl buffer.

2.4. Exo III -assisted cycling amplification

All oligonucleotides were denatured at 90 °C for 10 min and stored at 4 °C. The aptamer (0.2 μM) and different concentrations of OTA were mixed in 10 mM Tris-HCl buffer (10 mM $MgCl_2$, 50 mM NaCl and 10 mM KCl; pH 7.4) at 37 °C for 1.5 h. After the reaction, cDNA (0.2 μM), dsDNA (DNA-1 was hybridized with DNA-2) and 20 U Exo III were added into the above solution at 37 °C for 2 h. Finally, the solution was heated to 80 °C 10 min to stop the reaction.

2.5. Fabrication of the core-satellite sensor and SERS detection of OTA

We have prepared the SERS substrate according to the previously reported procedure [36,37]. Silicon (Si) substrate (5 mm × 5 mm) was pretreated using piranha solution (30% H_2O_2 mixed with concentrated H_2SO_4 at 1:3) at 60 °C for 15 min. After washing with water, the cleaned Si substrate was submersed into a 10% ethanolic APTES solution for 2 h. The substrate was washed with ethanol, and water for three times, respectively, and dried at 60 °C for 2 h. The substrate was subsequently immersed into 100 nm Au NPs solution for 12 h. After careful washing with water, the substrate was treated with 0.1 M aqueous solution of EDC and 1% PEG-COOH aqueous solution for 6 h, and the excess amino groups were reacted to prevent non-specific adsorption of Au NPs on the Si substrate. Next, DNA-S1 in Tris-HCl (10 mM) solution was added to DTT to activate the thiol-modified DNA-S1. The above PEG-COOH treated AuNPs modified substrate was immersed in DNA-S1 solution at room temperature overnight and washed with Tris-HCl (10 mM) to reduce non-specific interaction between Au NPs and DNA-S1. The obtained Si substrate was modified with Au NP-DNA-S1. Finally, the above substrate was stored in Tris-HCl solution (10 mM) at 4 °C.

The previously prepared SERS nanotag was added to the aforementioned Exo III amplified solution and kept at 37 °C for 2 h. After the hybridization process, the mixture was centrifuged (8000 rpm, 20 min), and the pellet was re-suspended in 10 mM Tris-HCl buffer. The SERS substrate modified with Au NPs-DNA-S1 was immersed in the above solution and kept at 37 °C for 4 h, and then fully hybridized to form core-satellite assemblies. Then carefully washed with water and dried for the final SERS detection analysis. The SERS measurement sample was scanned for 10 s with 633 nm laser 10% total laser power (the Renishaw in Via-Reflex micro-Raman spectrometer, 22.5 mW). At least 10 spots of the same sample were taken, and the averaged value of the spectra was taken for conclusive analysis.

After optimization testing, the OTA detection was performed under optimum conditions. A series of different concentrations OTA standard solutions were prepared to study the relationship between the OTA concentration and the SERS analysis intensity for ensuring the potential detection of OTA.

3. Results and discussion

3.1. Principle of sensor

Scheme 1 describes the principle of the proposed SERS sensor. Core-satellite assemblies were fabricated based on a DNA-driven self-assembly method. The large-size core Au NP was modified with DNA-S1 immobilized on a Si wafer. On the other side, Raman reporter molecule attached Au NP satellites were modified with DNA-S2. Firstly, OTA was added to completely react with the excess aptamer, and then cDNA was added with the same concentration as the aptamer. When introducing OTA into the sensing platform, the cDNA prefers to form the aptamer-OTA complex. In order to improve the binding efficiency of OTA and aptamer, OTA and the excess aptamer react first, and then cDNA was added to react with the remaining aptamer. Because the initial concentration of cDNA and the initial concentration of aptamer in the system are equal and can form double-stranded DNA, after the cDNA reacting with the remaining aptamer, the remaining cDNA can indicate the concentration of OTA and trigger the next reaction. Therefore, one part of cDNA hybridized with the remaining aptamer, and the other part of cDNA partly hybridized with dsDNA results in the formation of 3′ overhang end of the specific recognition site of Exo III. Then Exo III digests cDNA-dsDNA from the 3′-end of DNA-1, thus releasing cDNA and DNA-2. The released cDNA involves subsequent cycles, which giving rise to the formation of DNA-2. In the process of forming the core-satellite assemblies, a sandwich hybridization strategy was applied. DNA-2 is the linker of core-satellite assemblies, and the SERS intensity is direct proportional to the quantity of satellite Au NPs around the core Au NPs that resulted in significant increase of SERS responses with respect to the concentrations of OTA in the proposed system.

3.2. Characterization of SERS nanotag

As shown in Fig. 1, Au NPs have a diameter of 25 nm (Figs. 1A) and 100 nm (Fig. 1B), prepared according to previously published method [33,35]. After modification of DNA-S2, the absorption spectra of 25 nm Au NPs was red shifted about 4 nm to the preceding Au NPs (Fig. 1C). It was owing to the refractive index variation around the surface of Au NPs [38,39]. Scanning electron microscopy (SEM) analysis displays the existence of 100 nm Au NPs on the Si substrate (Fig. 1D).

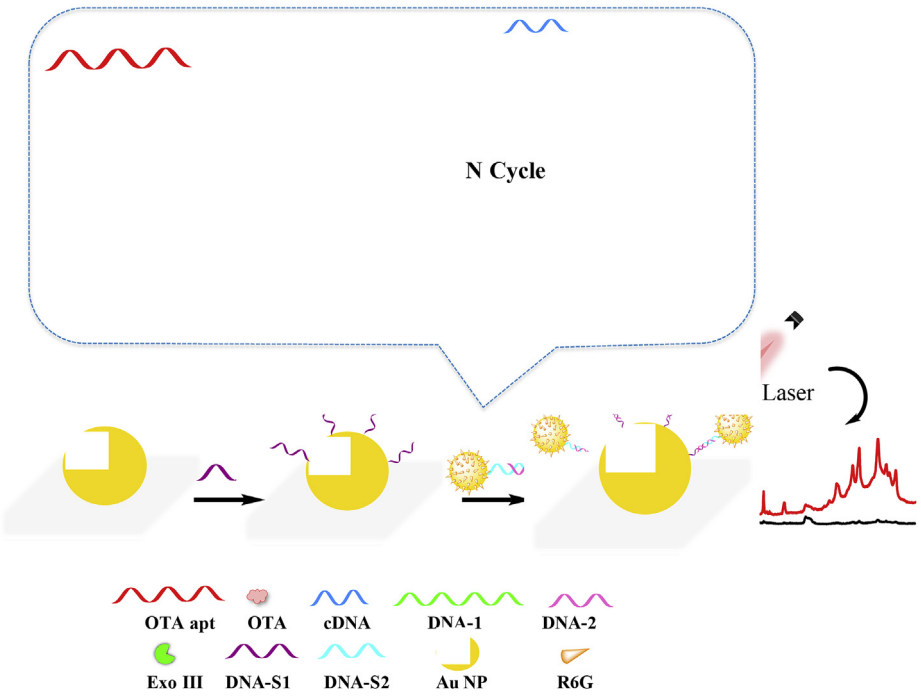

Scheme 1. Schematic illustration showing the working principle of SERS sensor for the detection of OTA.

3.3. Feasibility validation

In order to verify the feasibility of the SERS sensor, the SERS intensity of the system was further tested. Fig. 2A showed that a negligible Raman signal of the SERS substrate was detected without the target OTA, which indicates that the core-satellite assemblies cannot be formed. When OTA was then added into the system, the noticeable Raman signal of corresponding Raman reporter (R6G) was observed. The main characteristic peaks of R6G were observed at 613 cm^{-1}, 771 cm^{-1}, 1182 cm^{-1}, 1362 cm^{-1}, and 1511 cm^{-1}. The

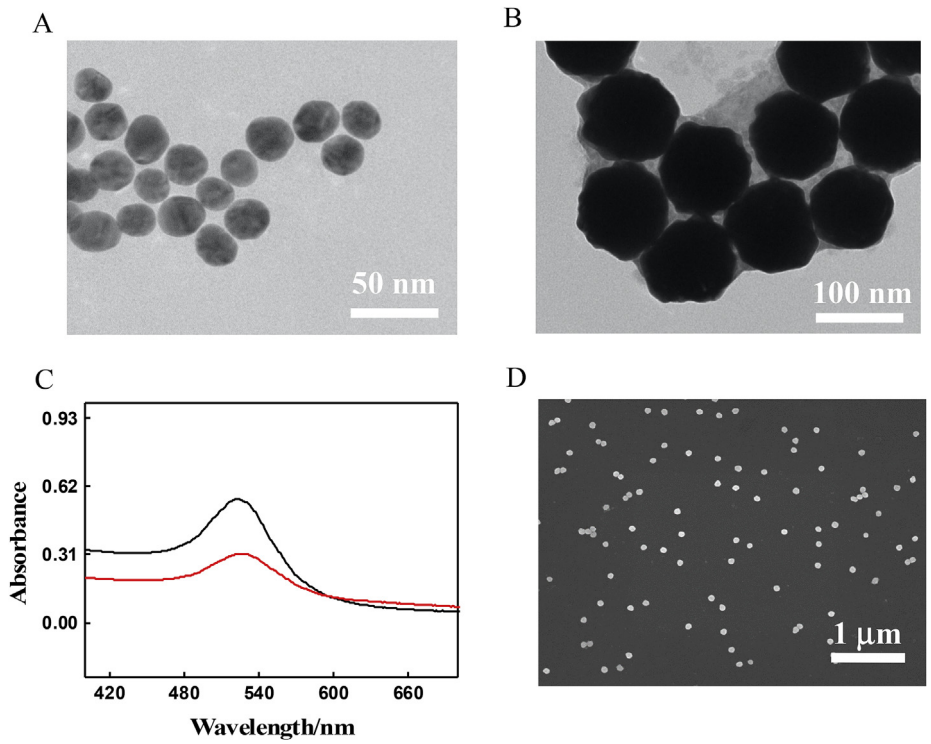

Fig. 1. (A) TEM images of 25 nm Au NPs. (B) TEM images of 100 nm Au NPs. (C) UV–vis spectra obtained for 25 nm Au NPs (C: black line) and Au NP-DNA-S2 (C: red line). (D) SEM image displaying the assembly of Au NPs on the Si substrate. (For interpretation of the references to color in this figure legend, the reader is referred to the Web version of this article.)

peaks at 613 cm^{-1} corresponds to the *C*—C—C in-plane vibration of the R6G molecule [40]. The peaks located at 771 $cm^{-1}$and 1182 cm^{-1} were attributed to the out-of-plane and in-plane vibrations of *C*—H bond. The peaks observed at 1362 cm^{-1}, 1511 cm^{-1} and 1648 cm^{-1} can be concerned with the aromatic *C*—C stretching vibration mode [41]. The characteristic band of R6G observed at 613 cm^{-1} served as a reference quantitative peak to assess the SERS sensitivity. This showed that the presence of OTA in the sensing platform, undergo Exo III -assisted recycling amplification, which thus released DNA-2, from recycling step, and acted as the linker for core-satellite assemblies. In the proposed SERS sensor, the Exo III -assisted cycling amplification for effective formation of core-satellite assemblies. The process of Exo III -assisted cycling amplification was investigated by polyacrylamide gel electrophoresis, as shown in Fig. 2B. By comparing lane H and lane I, it was found that the uppermost band disappeared after adding Exo III. It was owing to the digestion of cDNA-dsDNA by Exo III from the 3′-end of DNA-1, and releasing cDNA and DNA-2. Next, the composition of the core-satellite assembly was verified by SEM characterization, as shown in Fig. 2C and 2D. The addition of 25 ng mL^{-1} OTA into Au NPs displayed initiation of core-satellite assemblies (Fig. 2C), however well-defined core-satellite assemblies were formed at higher concentration of OTA (0.25 μg mL^{-1}; Fig. 2D), indicating that the concentration of OTA is crucial factor for progress of Au NPs core-satellite assemblies.

3.4. Optimization of the experiment conditions

The concentration of DNA-2 at hybridization with DNA-1 plays a vital role in the performance of the devised SERS sensor. Low concentration of DNA-2 might cause reduced SERS signals, whereas excess amount of DNA-2 might lead to an enhanced SERS signals. As shown in Fig. 3A, the detected SERS signal increased stage by stage while increasing the concentrations of DNA-2 in the range from 0.8 to 4.0 μM; at the same time, the concentration of DNA-1 was fixed on 2.0 μM. Notably, if the concentration of DNA-2 was more than 3.0 μM, the background signal was enhanced. Therefore, 2.0 μM DNA-2 was selected for subsequent determination.

The target reaction time closely associated with not only the formation of OTA-aptamer complex, but also the aptamer hybridization with cDNA and Exo III -assisted recycle. Fig. 3B showed that the SERS signals were increased from 30 to 90 min with respect to the target reaction time, and the reaction time became stable. Thus, optimal 90 min was selected as reaction time in this work. To access to the best assembly efficiency, the formation time of the core-satellite assemblies has also been optimized. As shown in Fig. 3C, the SERS signals gained gradually with the increasing of the reaction time and leveled out while 4 h of assembly time. Thus, we have selected 4 h as an optimized condition in this study.

3.5. Detection of OTA

The OTA was detected based on the above optimum conditions. The characteristic R6G SERS peak appeared at 613 cm^{-1} served as reference for the quantitative analysis of OTA. Fig. 4 showed that SERS spectra of different concentrations of OTA was recorded using core-shell satellite assembly substrate. The standard curve was plotted using SERS intensities at 613 cm^{-1} against the logarithmic concentration of OTA in the range of 0.0025 pg mL^{-1} to 0.25 ng mL^{-1}, the correlation coefficient (R^2) of 0.9739 and the limit of detection (LOD) of OTA was 0.83 fg mL^{-1} (S/N = 3). The obtained LOD was highly comparable with the other previously reported OTA sensors as shown in Table 1 [32,42–46]. Such very low LOD of OTA was achieved mainly because of the excellent Exo III -assisted recycling amplification strategy, as well as highly SERS activity of core-satellite assemblies.

3.6. Specificity and uniformity of the SERS sensor

To check into the selectivity of this proposed approach, the mycotoxins such as AFB1, ZEN and OTB were selected and tested

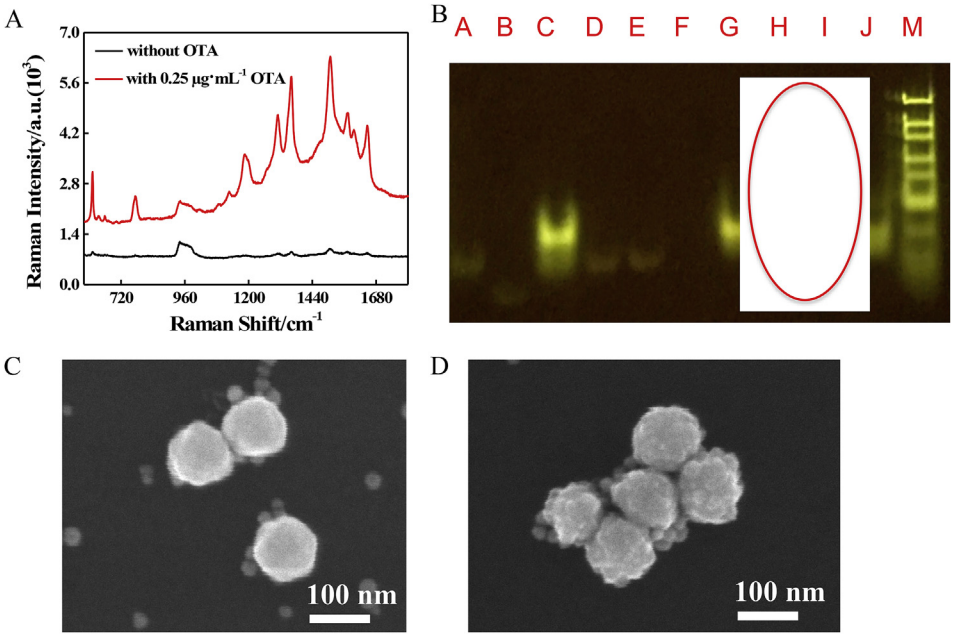

Fig. 2. (A) SERS spectra obtained for R6G on core–satellite assemblies without OTA (A: black line) and with 0.25 μg mL^{-1} OTA (A: red line). (B) The image of polyacrylamide gel electrophoresis. Line A - DNA-1; Line B - DNA-2; Line C - DNA-1+DNA-2; Line D - OTA apt; Line E – OTA apt + OTA; Line F - cDNA; Line G - OTA apt + OTA + cDNA; Line H - OTA apt + OTA + cDNA + DNA-1 + DNA-2; Line I - OTA apt + OTA + cDNA + DNA-1+ DNA-2+ Eox III; Line J - OTA apt + cDNA + DNA-1 + DNA-2 + Exo III. (C) SEM images of Au NPs core-satellite assemblies with 25 ng mL^{-1} OTA. (D) SEM images of Au NPs core-satellite assemblies with 0.25 μg mL^{-1} OTA. (For interpretation of the references to color in this figure legend, the reader is referred to the Web version of this article.)

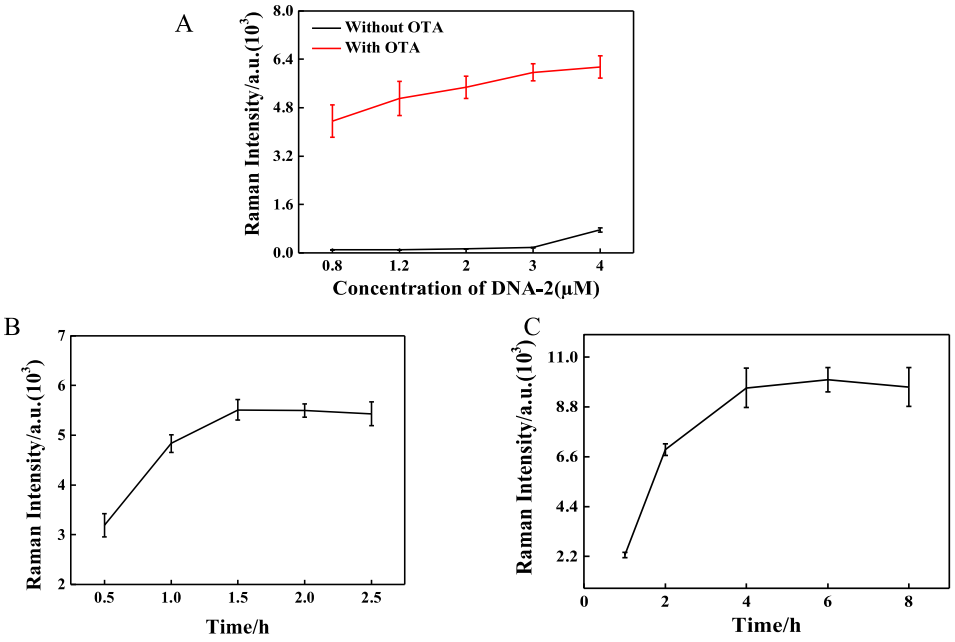

Fig. 3. (A) Optimization of OTA detection: the effect of DNA-2 concentration, (B) reaction time for the assembly of OTA target, (C) and time for the formation of Au NPs core-satellite assemblies.

under same experimental conditions. Meanwhile, 0.025 ng mL^{-1} OTA, the control sample (without any OTA target) and the above interference mycotoxins (5.0 ng mL^{-1}) were added. As shown in Fig. 5A, although the concentration of other mycotoxins was about 200-fold higher than OTA, no notable SERS signal of these mycotoxins were observed. Moreover, when compared with the control, the presence of OTA was markedly increasing SERS signal, which verified the high specificity of the proposed Exo III -assisted core-satellite assembly approach based detection of OTA. To inquire into the uniformity of the SERS substrate, 10 random sites in the SERS substrate were selected and detected the Raman signals as shown in Fig. 5B, the results evidenced that the intensity deviation was about within 10% that demonstrating the good uniformity of the core-satellite assembly substrate.

3.7. *Application of the SERS sensor to detect OTA in red wine sample*

To verify the practicability, the proposed approach was used in detecting OTA in actual sample, with red wine as a reagent sample, for the recovery determination for the detection of OTA (0.25 ng mL^{-1}, 5.0 ng mL^{-1}, and 25.0 ng mL^{-1}). Table 2 showing the recovery results of OTA detection in red wine samples. The recovery was within the range of 95.9–105.7%, and the corresponding relative standard deviation (RSD) was between 6.08–8.61%, demonstrating that the proposed SERS sensor can be potentially utilized for detecting OTA in real samples for food safety and clinical applications.

4. Conclusions

In summary, a high performance SERS sensor is developed based on core-satellite assemblies and exonuclease assisted double amplification strategy. The proposed double amplification strategy consists with the following two aspects: (i) Exo III induced signal amplification: in the presence of the target molecules, Exo III could efficiently produce a large amount of linkers

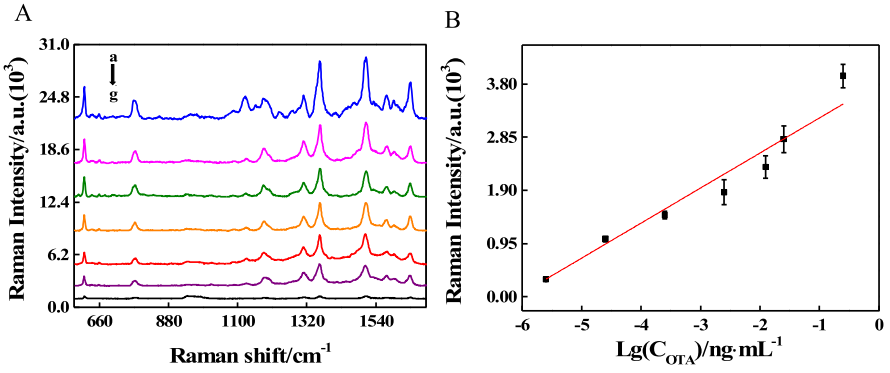

Fig. 4. (A) Raman spectra obtained for different concentration of OTA using Au NPs core–satellite assemblies substrate (curves a–g: 2.50 × 10^{-3} ng mL^{-1} to 25 ng mL^{-1}), (B) and corresponding linear calibration plot obtained by plotting Raman intensity at 613 cm^{-1} versus logarithmic concentrations of OTA.

Table 1
Comparison of proposed OTA detection with other approaches in terms of dynamic range and LOD.

Method	Dynamic rang	LOD	Ref
Electrochemical	0.001–0.5 ng mL^{-1}	0.26 pg mL^{-1}	Wei and Zhang, 2018
	0.1 pg mL^{-1}–10 ng mL^{-1}	39 fg mL^{-1}	Zhang et al., 2018
Colorimetric	0.05–2.0 ng mL^{-1}	0.023 ng mL^{-1}	Lin et al., 2017
Fluorescent	0.08–200 ng mL^{-1}	0.08 ng mL^{-1}	Wu et al., 2018
	0.01–50 ng mL^{-1}	0.004 ng mL^{-1}	Shao et al., 2018
SERS	1.20 pg mL^{-1}–3.31 μg mL^{-1}	0.48 pg mL^{-1}	Sony et al., 2018
	0.0025 pg mL^{-1}–0.25 ng mL^{-1}	0.83 fg mL^{-1}	This work

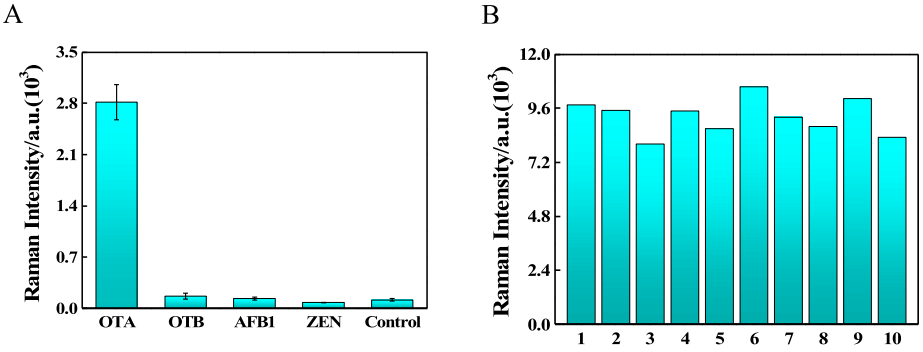

Fig. 5. (A) Selectivity towards the detection of OTA using Au NPs core–satellite assemblies substrate. The concentration of OTA was 0.025 ng mL^{-1} and the concentration of other compounds such as OTB, AFB1, ZEN, and control samples were of 5 ng mL^{-1}. (B) Raman spectra were collected at 10 randomly selected spots on the Au NPs core–satellite assemblies substrate. The Raman intensity was referenced at 613 cm^{-1} used for drawing the bar plots. The RSD of the above analysis was about 7.88%.

Table 2
The recovery table showing the detection of OTA in red wine samples (n = 3).

Sample	OTA added (ng/mL)	Total found (ng/mL)	Recovery (%)	RSD (%)
1	0.25	0.2395	95.9	6.08
2	5	5.078	101.6	8.61
3	25	26.42	105.7	6.81

to assemble the core-satellite Au NP nanostructure; (ii) Core-satellite assemblies induced signal amplification: The formation of Au NP core-satellite nanostructures would create numerous SERS "hot-spots", which would significantly enhance the Raman signals. The practical usage of the proposed sensing strategy was demonstrated to detect OTA with the RSDs values of 6.08–8.61%, and a LOD of 0.83 fg mL^{-1} (S/N = 3) in red wine. Finally, this double amplification strategy could be potentially utilized for the detection of other DNA specific targets, for example, oligonucleotides, miRNAs, and other DNA aptamer targeted molecules. Thus, it could find tremendous potential applications in both food safety and clinical diagnosis.

Declaration of competing interest

The authors declare that they have no known competing financial interests or personal relationships that could have appeared to influence the work reported in this paper.

CRediT authorship contribution statement

Dandan Huang: Validation, Formal analysis, Conceptualization, Methodology, Investigation, Data curation, Writing - original draft, Visualization. **Jiaming Chen:** Writing - review & editing. **Li Ding:** Formal analysis, Investigation. **Fang Luo:** Supervision. **Bin Qiu:** Supervision.

Acknowledgement

This work was supported by the National Natural Science Foundation of China (21675028), the Key Research and Development Program of Zhejiang Province (2020C02022); the Cooperative Project of Production and Study in University of Fujian Province (2018Y4007); STS Key Project of Fujian Province (2017T3007); Nature Sciences Funding of Fujian Province (2018J01682); and the Program for New Century Excellent Talents in Fujian Province University.

References

[1] J. Chen, L. Guo, B. Qiu, Z. LinT. Wang, Application of ordered nanoparticle self-assemblies in surface-enhanced spectroscopy, Materials Chemistry Frontiers 2 (2018) 835–860.
[2] C.L. Haynes, A.D. McFarlandR, P.V. Duyne, Surface-enhanced Raran Spectroscopy, Anal. Chem. (2005) 338A–346A.
[3] S. Schlucker, Surface-enhanced Raman spectroscopy: concepts and chemical applications, Angew. Chem., Int. Ed. Engl. 53 (2014) 4756–4795.
[4] J. Chen, Y. Huang, P. Kannan, L. Zhang, Z. Lin, J. Zhang, T. Chen, L. Guo, Flexible and adhesive surface enhance Raman scattering active tape for rapid detection of pesticide residues in fruits and vegetables, Anal. Chem. 88 (2016) 2149–2155.
[5] S.Y. Ding, E.M. You, Z.Q. Tian, M. Moskovits, Electromagnetic theories of surface-enhanced Raman spectroscopy, Chem. Soc. Rev. 46 (2017) 4042–4076.
[6] R. Matthew, X. Xiaohu, C.H. Moran, Z. Fei, Q. Dong, L. Zhi-Yuan, X. Younan, Generation of hot spots with silver nanocubes for single-molecule detection by surface-enhanced Raman scattering, Angew. Chem. 50 (2011) 5473–5477.
[7] Z.Q. Tian, B. RenD, Y. Wu, Surface-enhanced Raman scattering: from noble to transition metals and from rough surfaces to ordered nanostructures, J. Phys. Chem. B 106 (2002) 9463–9483.
[8] B. Lin, J. Chen, P. Kannan, Y. Zeng, B. Qiu, L. Guo, Z. Lin, Rapid synthesis of a highly active and uniform 3-dimensional SERS substrate for on-spot sensing of dopamine, Microchimica Acta 186 (2019) 260.
[9] J.M. Chen, L.H. Guo, B. Qiu, Z.Y. Lin, T. Wang, Application of ordered nanoparticle self-assemblies in surface-enhanced spectroscopy, Materials Chemistry Frontiers 2 (2018) 835–860.
[10] L.G. Xu, M.Z. Sun, W. Ma, H. Kuang, C.L. Xu, Self-assembled nanoparticle dimers with contemporarily relevant properties and emerging applications, Mater Today Off. 19 (2016) 595–606.
[11] L.G. Xu, W.J. Yan, W. Ma, H. Kuang, X.L. Wu, L.Q. Liu, Y. Zhao, L.B. Wang,

C.L. Xu, SERS encoded silver pyramids for attomolar detection of multiplexed disease biomarkers, Adv. Mater. 27 (2015) 1706–1711.
[12] Q. Lidong, Z. Shengli, X. Can, A. Ariel, G.C. SchatzC, A. Mirkin, Designing, fabricating, and imaging Raman hot spots, Proc. Natl. Acad. Sci. U. S. A. 103 (2006) 13300–13303.
[13] H. Fu, J. Chen, L. Chen, X. Zhu, Z. Chen, B. Qiu, Z. Lin, L. Guo, G. Chen, A calcium alginate sponge with embedded gold nanoparticles as a flexible SERS substrate for direct analysis of pollutant dyes, Microchimica Acta 186 (2019) 64.
[14] A. Li, L. Tang, D. Song, S. Song, W. Ma, L. Xu, H. Kuang, X. Wu, L. Liu, X. Chen, A SERS-active sensor based on heterogeneous gold nanostar core-silver nanoparticle satellite assemblies for ultrasensitive detection of aflatoxinB1, Nanoscale 8 (2016) 1873.
[15] X. Liguang, Y. Wenjing, M. Wei, K. Hua, W. Xiaoling, L. Liqaing, Z. Yuan, W. Libing, X. Chuanlai, Biosensors: SERS encoded silver pyramids for attomolar detection of multiplexed disease biomarkers (Adv. Mater. 10/2015), Adv. Mater. 27 (2015) 1706–1711.
[16] Y.Y. Li, Q.C. Zhao, Y.D. Wang, T.T. Man, L. Zhou, X. Fang, H. Pei, L.F. Chi, J. Liu, Ultrasensitive signal-on detection of nucleic acids with surface-enhanced Raman scattering and exonuclease III-assisted probe amplification, Anal. Chem. 88 (2016) 11684–11690.
[17] L. Reddy, K. Bhoola, Ochratoxins—food contaminants: impact on human health, Toxins 2 (2010) 771–779.
[18] T.R. Bui-Klimke, F. Wu, Ochratoxin A and human health risk: a review of the evidence, Crit. Rev. Food Sci. Nutr. 55 (2015) 1860–1869.
[19] A. Valero, S. Marin, A.J. Ramos, V. Sanchis, Survey: Ochratoxin A in European special wines, Food Chem. 108 (2008) 593–599.
[20] K.J. Van der Merwe, P.S. Steyn, L. Fourie, Mycotoxins II. The constitution of ochratoxins A, B, and C, metabolites of Aspergillus ochraceus wilh, Journal of the Chemical Society. Perkin transactions 1 (1965) 7083–7088.
[21] J.W. BennettM, Mycotoxins Klich, Clin. Microbiol. Rev. 16 (2003), 497-+.
[22] R. Chauhan, J. Singh, T. Sachdev, T. BasuB, D. Malhotra, Recent advances in mycotoxins detection, Biosens. Bioelectron. 81 (2016) 532–545.
[23] Y.F. Tao, S.Y. Xie, F.F. Xu, A.M. Liu, Y.X. Wang, D.M. Chen, Y.H. Pan, L.L. Huang, D.P. Peng, X. WangZ, H. Yuan, Ochratoxin A: Toxicity, oxidative stress and metabolism, Food Chem. Toxicol. 112 (2018) 320–331.
[24] M. Zhao, P. Wang, Y. Guo, L. Wang, F. Luo, B. Qiu, L. Guo, X. Su, Z. Lin, G. Chen, Detection of aflatoxin B1 in food samples based on target-responsive aptamer-cross-linked hydrogel using a handheld pH meter as readout, Talanta 176 (2018) 34–39.
[25] A. el Khoury, A. Atoui, Ochratoxin A: General overview and actual molecular status, Toxins 2 (2010) 461–493.
[26] H.B. Bostan, N.M. Danesh, G. Karimi, M. Ramezani, S.A.M. Shaegh, K. Youssefi, F. Charbgoo, K. AbnousS, M. Taghdisi, Ultrasensitive detection of ochratoxin A using aptasensors, Biosens. Bioelectron. 98 (2017) 168–179.
[27] C. Armutcu, L. Uzun, A. Denizli, Determination of Ochratoxin A traces in foodstuffs: comparison of an automated on-line two-dimensional high-performance liquid chromatography and off-line immunoaffinity-high-performance liquid chromatography system, J. Chromatogr. A 1569 (2018) 139–148.
[28] L. Campone, A.L. Piccinelli, R. Celano, I. Pagano, M. Russo, L. Rastrelli, Rapid and automated on-line solid phase extraction HPLC-MS/MS with peak focusing for the determination of ochratoxin A in wine samples, Food Chem. 244 (2018) 128–135.
[29] Z.C. Sun, J.W. Lv, X. Liu, Z.W. Tang, X.R. Wang, Y. XuB, D. Hammock, Development of a nanobody-AviTag fusion protein and its application in a streptavidin-biotin-amplified enzyme-linked immunosorbent assay for ochratoxin A in cereal, Anal. Chem. 90 (2018) 10628–10634.
[30] E.-O. Ganbold, C.M. Lee, E.-M. Cho, S.J. Son, S. Kim, S.-W. JooS, I. Yang, Subnanomolar detection of ochratoxin A using aptamer-attached silver nanoparticles and surface-enhanced Raman scattering, Analytical Methods 6 (2014).
[31] Y. Zhao, Y. Yang, Y. Luo, X. Yang, M. Li, Q. Song, Double detection of mycotoxins based on SERS labels embedded Ag@Au core-shell nanoparticles, ACS Appl. Mater. Interfaces 7 (2015) 21780–21786.
[32] D. Song, R. Yang, S. Fang, Y. Liu, F. Long, A. Zhu, SERS based aptasensor for ochratoxin A by combining Fe3O4@Au magnetic nanoparticles and Au-DTNB@Ag nanoprobes with multiple signal enhancement, Mikrochim. Acta 185 (2018) 491.
[33] G. Frens, Z. Kolloid, J. Turkevich, J. Hillier, P.C. Stevenson, Controlled Nucleation for the Regulation of the Particle Size in Monodisperse Gold Suspensions, Natrue, 1972.
[34] X. Cui, Y. Huang, J. Wang, L. Zhang, Y. Rong, W. Lai, T. Chen, A remarkable sensitivity enhancement in a gold nanoparticle-based lateral flow immunoassay for the detection of Escherichia coli O157:H7, RSC Adv. 5 (2015) 45092–45097.
[35] J. Niu, T. Zhu, Z. Liu, One-step seed-mediated growth of 30–150 nm quasi-spherical gold nanoparticles with 2-mercaptosuccinic acid as a new reducing agent, Nanotechnology 18 (2007) 325607.
[36] N.H. Kim, S.J. Lee, M. Moskovits, Reversible tuning of SERS hot spots with aptamers, Adv. Mater. 23 (2011) 4152–4156.
[37] L.H. Guo, G.N. ChenD, H. Kim, Three-dimensionally assembled gold nanostructures for plasmonic biosensors, Anal. Chem. 82 (2010) 5147–5153.
[38] D.F. Wang, Y.Y. Li, Z.Y. Lin, B. QiuL, H. Guo, Surface-enhanced electrochemiluminescence of Ru@SiO2 for ultrasensitive detection of carcinoembryonic antigen, Anal. Chem. 87 (2015) 5966–5972.
[39] L.H. Guo, A.R. Ferhan, K. LeeD, H. Kim, Nanoarray-based biomolecular detection using individual Au nanoparticles with minimized localized surface plasmon resonance variations, Anal. Chem. 83 (2011) 2605–2612.
[40] K. Zhang, T. Zeng, X. Tan, W. Wu, Y. Tang, H. Zhang, A facile surface-enhanced Raman scattering (SERS) detection of rhodamine 6G and crystal violet using Au nanoparticle substrates, Appl. Surf. Sci. 347 (2015) 569–573.
[41] Y.Q. Wang, S. Ma, Q.Q. Yang, X.J. Li, Size-dependent SERS detection of R6G by silver nanoparticles immersion-plated on silicon nanoporous pillar array, Appl. Surf. Sci. 258 (2012) 5881–5885.
[42] T. Zhang, B. Xing, Q. Han, Y. Lei, D. Wu, X. Ren, Q. Wei, Electrochemical immunosensor for ochratoxin A detection based on Au octahedron plasmonic colloidosomes, Anal. Chim. Acta 1032 (2018) 114–121.
[43] B. Shao, X. Ma, S. Zhao, Y. Lv, X. Hun, H. Wang, Z. Wang, Nanogapped Au(core) @ Au-Ag(shell) structures coupled with Fe3O4 magnetic nanoparticles for the detection of Ochratoxin A, Anal. Chim. Acta 1033 (2018) 165–172.
[44] C. Lin, H. Zheng, M. Sun, Y. Guo, F. Luo, L. Guo, B. Qiu, Z. Lin, G. Chen, Highly sensitive colorimetric aptasensor for ochratoxin A detection based on enzyme-encapsulated liposome, Anal. Chim. Acta 1002 (2018) 90–96.
[45] K. Wu, C. Ma, H. Zhao, M. Chen, Z. Deng, Sensitive aptamer-based fluorescence assay for ochratoxin A based on RNase H signal amplification, Food Chem. 277 (2019) 273–278.
[46] M. Wei, W. Zhang, Ultrasensitive aptasensor with DNA tetrahedral nanostructure for Ochratoxin A detection based on hemin/G-quadruplex catalyzed polyaniline deposition, Sensor. Actuator. B Chem. 276 (2018) 1–7.